Supplementary Material

for *Mourgela et al. "The radiative effect and climate responses of present-day wildfire emissions"*

Wildfire emissions analysis

Table S1: Regional contribution to the total global wildfire emissions (%) per species for 2015 (CMIP6 wildfire dataset, scenario SSP3-7.0 (Feng et al., 2020))

	BC	OC	NH_3	CO	SO_2	NO_x	NMVOCs
Boreal North America	3.7	8.2	8.6	5.3	6.6	1.1	5.7
Boreal & Central Asia	9.9	14.7	18.7	11.1	12.6	4.1	11.8
Africa	50.3	39.9	36.2	45.1	48.9	61.7	43.2
South America	16.5	15.3	15.7	15.2	13.2	14.8	14.9
Equatorial Asia	4.5	7.5	7.5	9.4	4.5	3.8	10.5
Other	15.1	14.3	13.3	13.9	14.3	14.5	14
Global (Tg)	**1.7**	**15.2**	**3.9**	**328**	**2.2**	**13.7**	**63.2**

Global emissions effect on pressure and winds | Atmosphere-only simulations and fully coupled ocean-atmosphere simulations

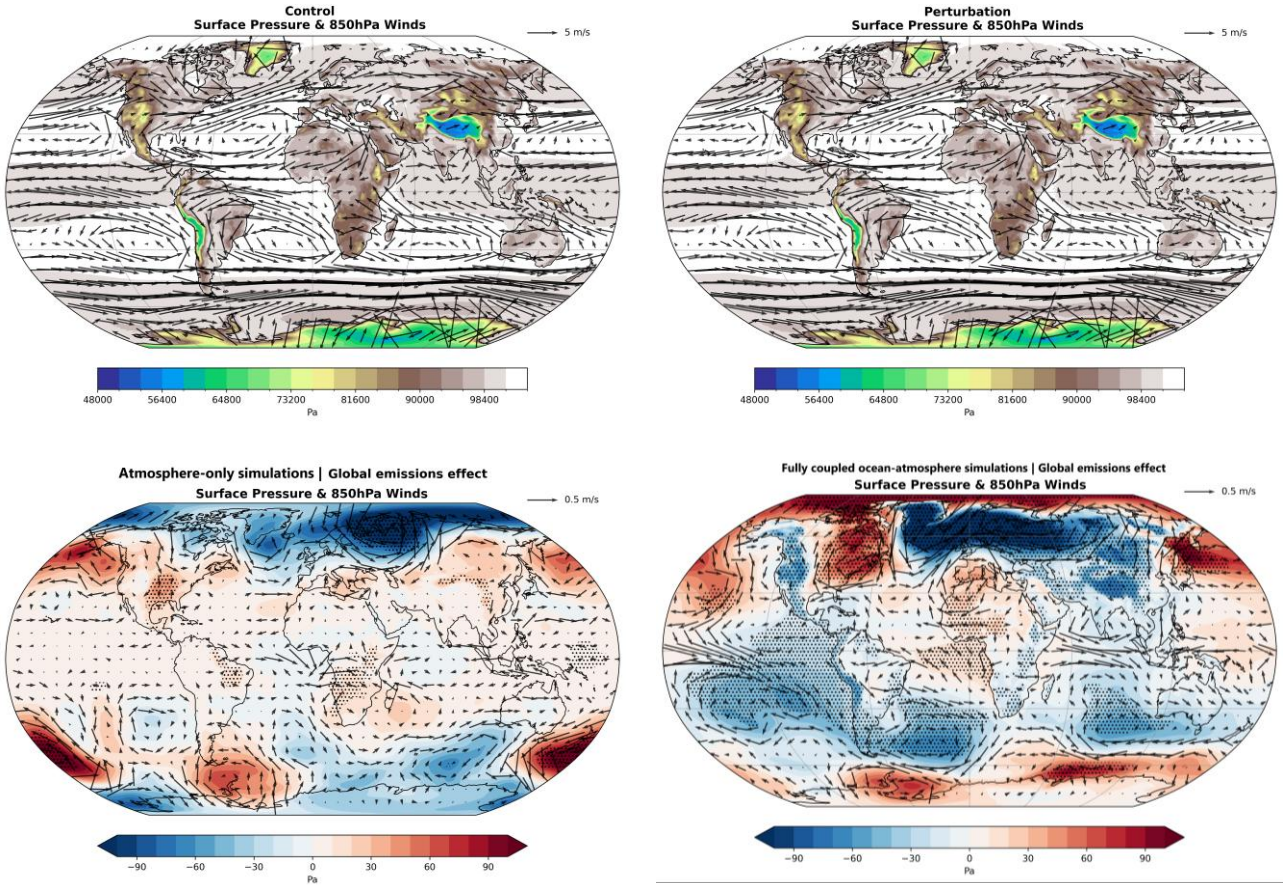

Figure S1: Spatial distribution of the surface pressure (Pa) along with wind direction and speed at 850hPa of the control simulation, the perturbation simulation, and their difference (30-year mean of the atmosphere-only simulations and 50-year mean of the fully coupled ocean-atmosphere simulations).

Global wildfire emissions effect on Africa and Southeast Atlantic Ocean

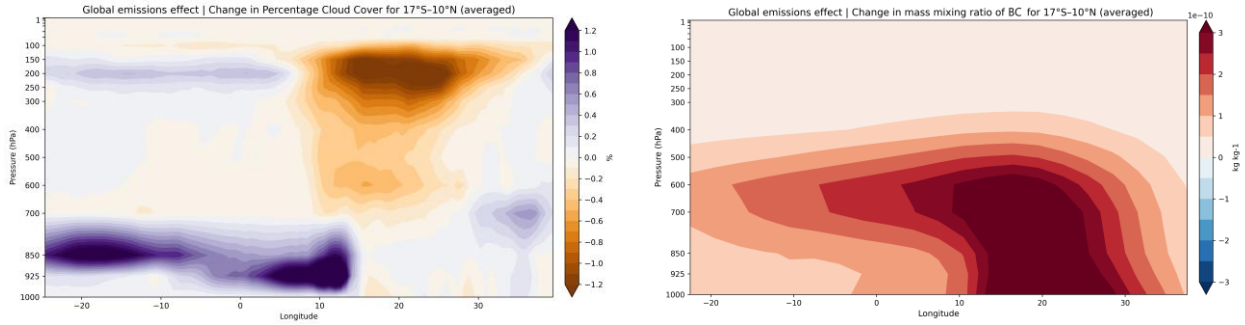

Figure S2: Vertical profiles of cloud cover (%) change and BC (black carbon) mass mixing ratio (kg/kg) increase due to the present-day wildfire emissions for the region of Africa and southeast Atlantic (red square). The profiles were calculated as the difference between the perturbation run and the control run (30 years of atmosphere-only simulations) depicting the synergistic effect of global wildfire emissions.

Global wildfire emissions effect on North Atlantic Ocean

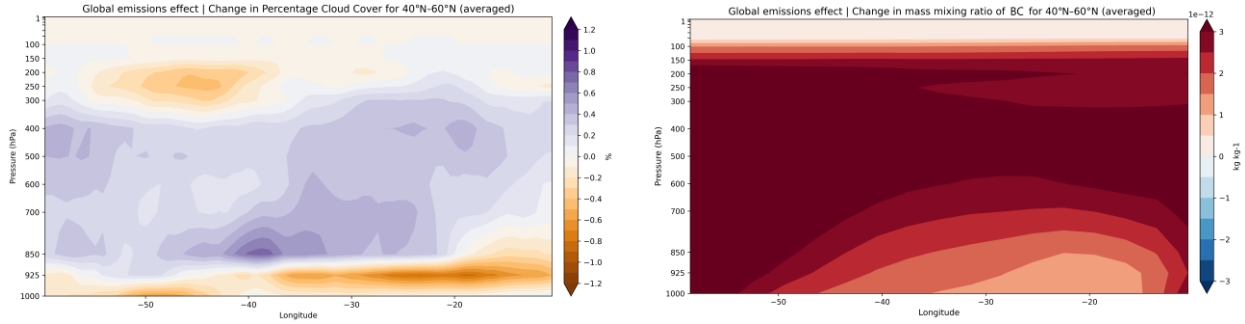

Figure S3: Vertical profiles of cloud cover (%) change and BC (black carbon) mass mixing ratio (kg/kg) increase due to the present-day wildfire emissions for the region of North Atlantic (red square). The profiles were calculated as the difference between the perturbation run and the control run (30 years of atmosphere-only simulations) depicting the synergistic effect of global wildfire emissions.

Global wildfire emissions effect on Indian Ocean

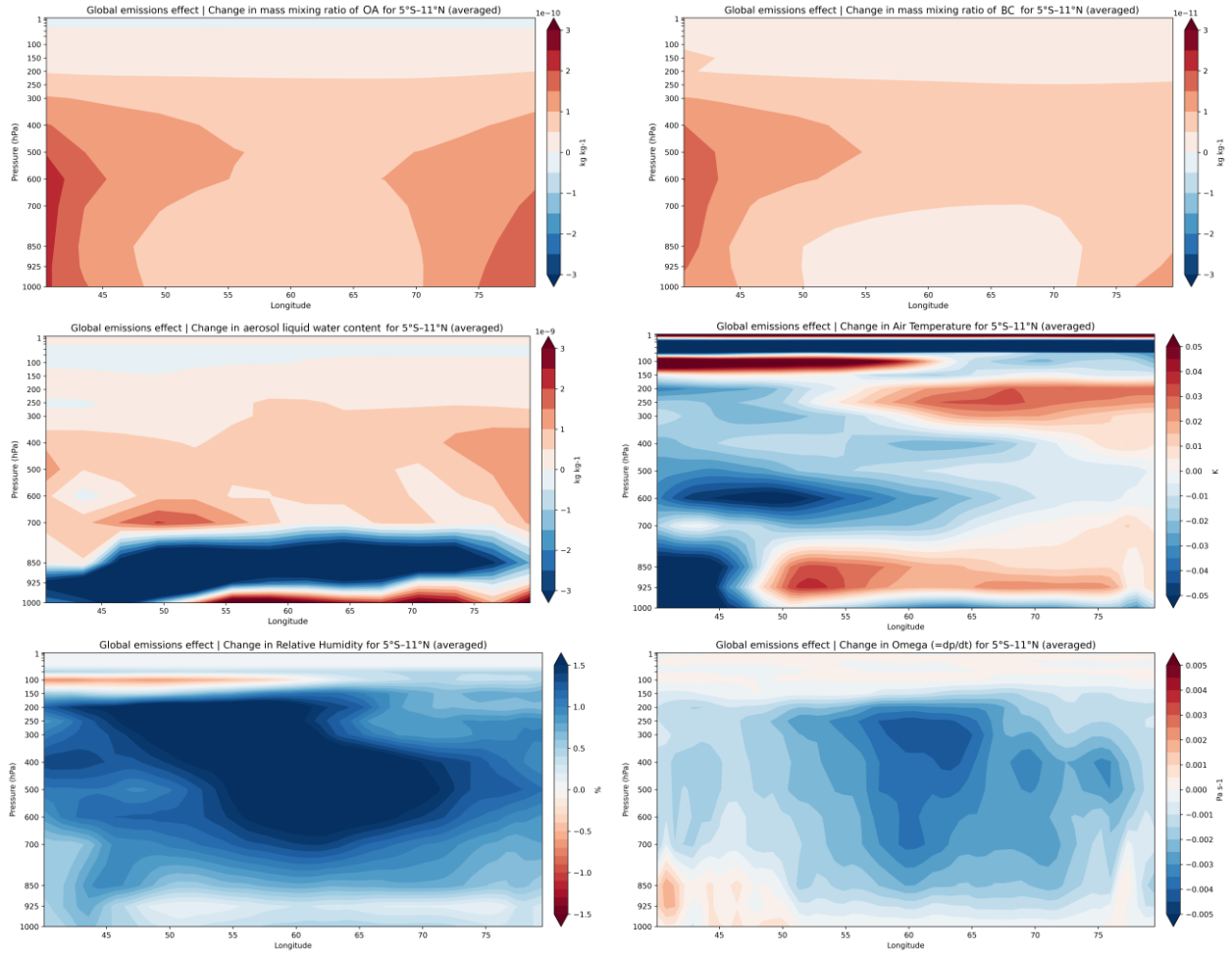

Figure S4: Vertical profiles of the changes in the mixing ratio (kg/kg) of BC (black carbon), OA (organic aerosols), aerosol liquid water content, and the changes in air temperature (K), relative humidity (%) and omega due to the present-day wildfire emissions for the region of Indian Ocean (red square). The profiles were calculated as the difference between the perturbation run and the control run (30 years of atmosphere-only simulations) depicting the synergistic effect of global wildfire emissions.

Regional wildfire emissions effects on global scale | Atmosphere-only simulations: Radiative Effect (RE), its decomposition and drivers

- **Boreal North America (BNA) emissions effects**

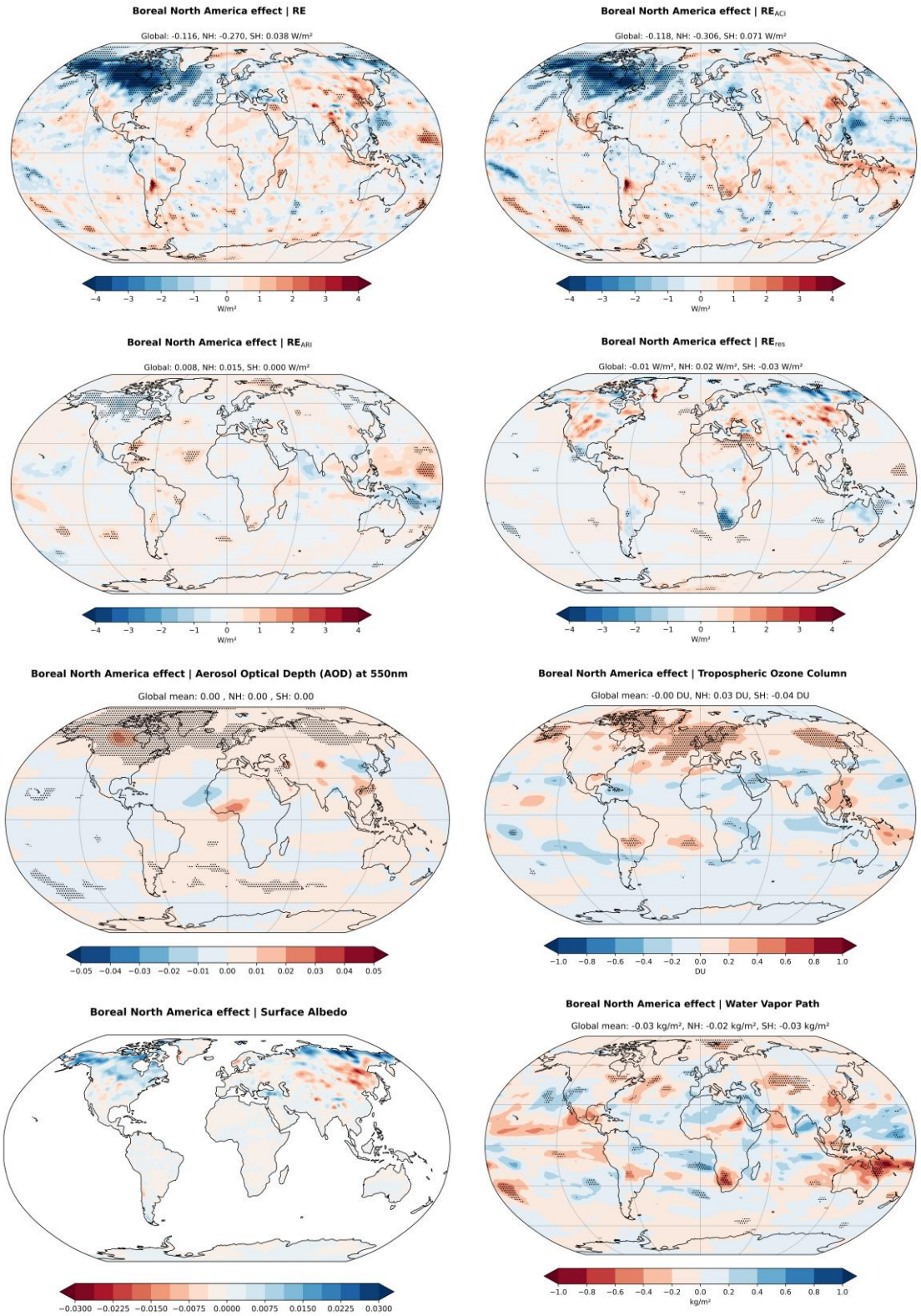

Figure S5: Spatial distribution of the Radiative Effect (RE) (W/m^2) of the present-day wildfire emissions from Boreal North America (BNA), and its decomposition into the RE due to the Aerosol-Radiation Interactions (RE_{ARI}), the Aerosol-Cloud Interactions (RE_{ACI}), and the residual term (RE_{res}). Moreover, the spatial distribution of the changes in Aerosol Optical Depth (AOD) at 500nm, the tropospheric O_3 (DU), the water vapor path (kg/m^2) and the surface albedo, are presented. The maps represent the difference between the 30-year mean of the atmosphere-only perturbation simulations and the 30-year mean of the simulations conducted without the BNA emissions. Black stippling denotes that the change is significant at the 0.05 level. It is noted that in the present work, surface albedo is determined as (Surface Upwelling Shortwave Radiation)/(Surface Downwelling Shortwave Radiation)

- **Boreal & Central Asia (BCA) emissions effects**

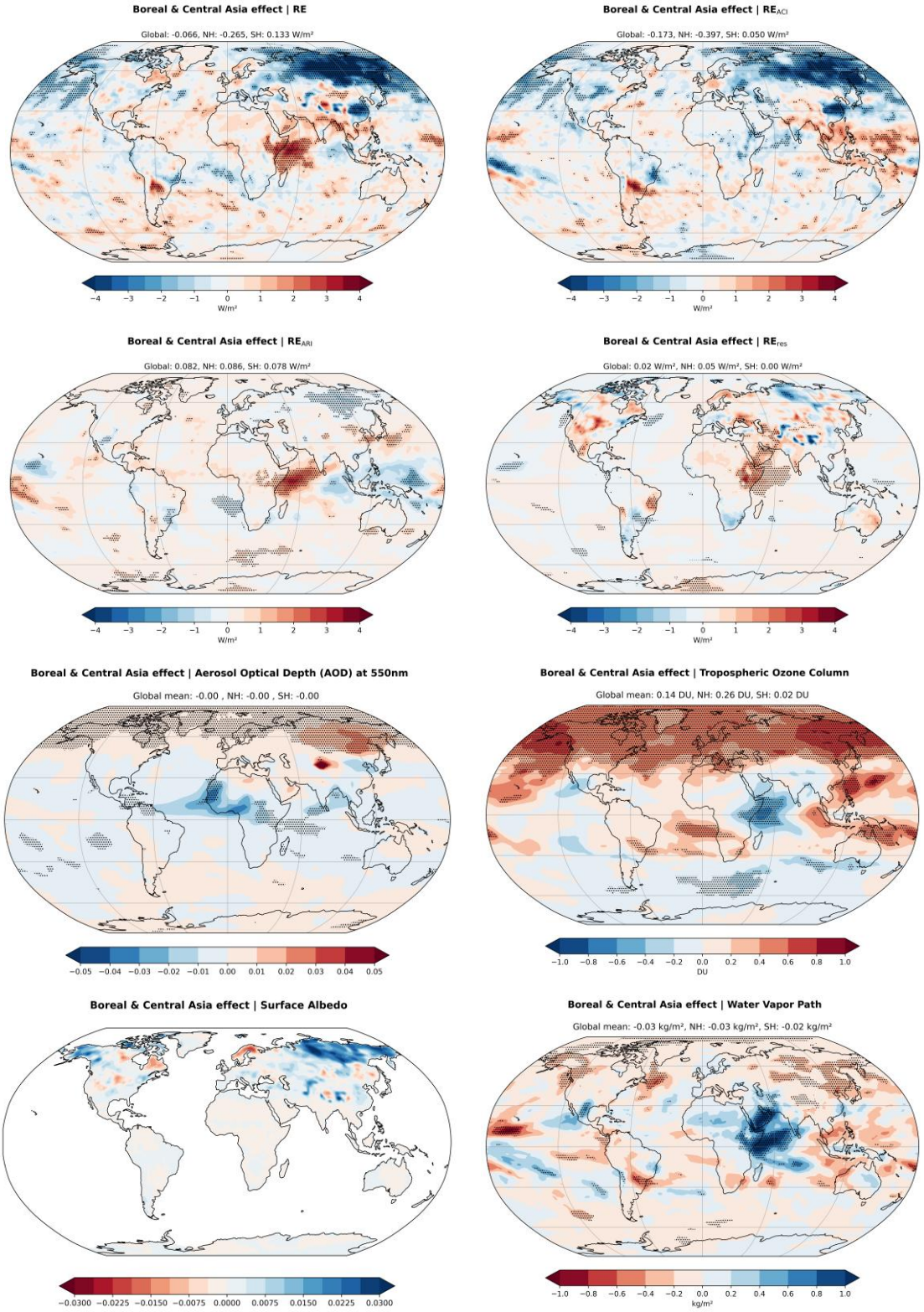

Figure S6: Spatial distribution of the Radiative Effect (RE) (W/m^2) of the present-day wildfire emissions from Boreal & Central Asia (BCA), and its decomposition into the RE due to the Aerosol-Radiation Interactions (RE_{ARI}), the Aerosol-Cloud Interactions (RE_{ACI}), and the residual term (RE_{res}). Moreover, the spatial distribution of the changes in Aerosol Optical Depth (AOD) at 500nm, the tropospheric O_3 (DU), the water vapor path (kg/m^2) and the surface albedo, are presented. The maps represent the difference between the 30-year mean of the atmosphere-only perturbation simulations and the 30-year mean of the simulations conducted without the BCA emissions. Black stippling denotes that the change is significant at the 0.05 level. It is noted that in the present work, surface albedo is determined as (Surface Upwelling Shortwave Radiation)/(Surface Downwelling Shortwave Radiation)

- **South America (SA) emissions effects**

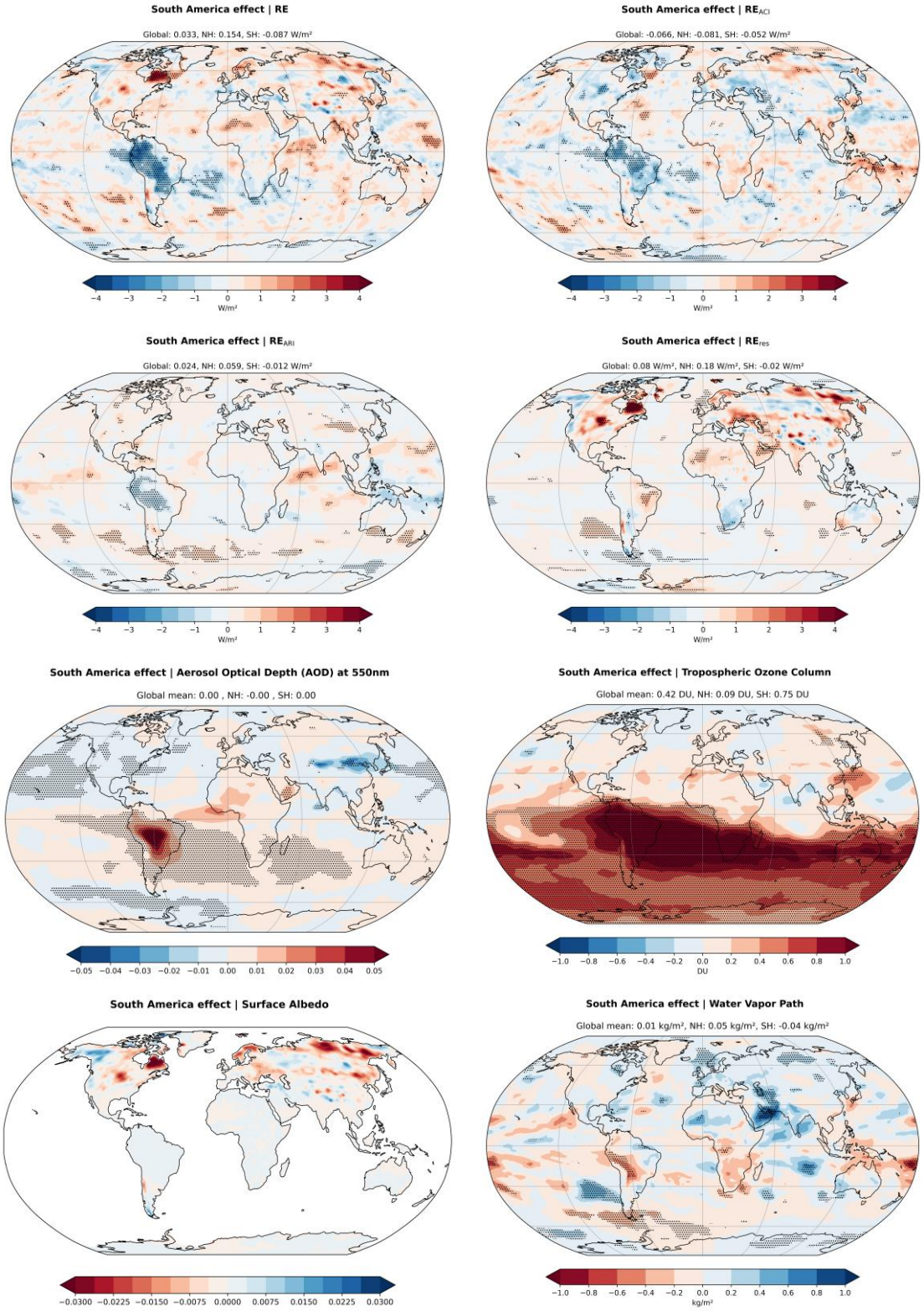

Figure S7: Spatial distribution of the Radiative Effect (RE) (W/m^2) of the present-day wildfire emissions from South America (SA), and its decomposition into the RE due to the Aerosol-Radiation Interactions (RE$_{ARI}$), the Aerosol-Cloud Interactions (RE$_{ACI}$), and the residual term (RE$_{res}$). Moreover, the spatial distribution of the changes in Aerosol Optical Depth (AOD) at 500nm, the tropospheric O_3 (DU), the water vapor path (kg/m^2) and the surface albedo, are presented. The maps represent the difference between the 30-year mean of the atmosphere-only perturbation simulations and the 30-year mean of the simulations conducted without the SA emissions. Black stippling denotes that the change is significant at the 0.05 level. It is noted that in the present work, surface albedo is determined as (Surface Upwelling Shortwave Radiation)/(Surface Downwelling Shortwave Radiation)

- **Africa (AF) emissions effects**

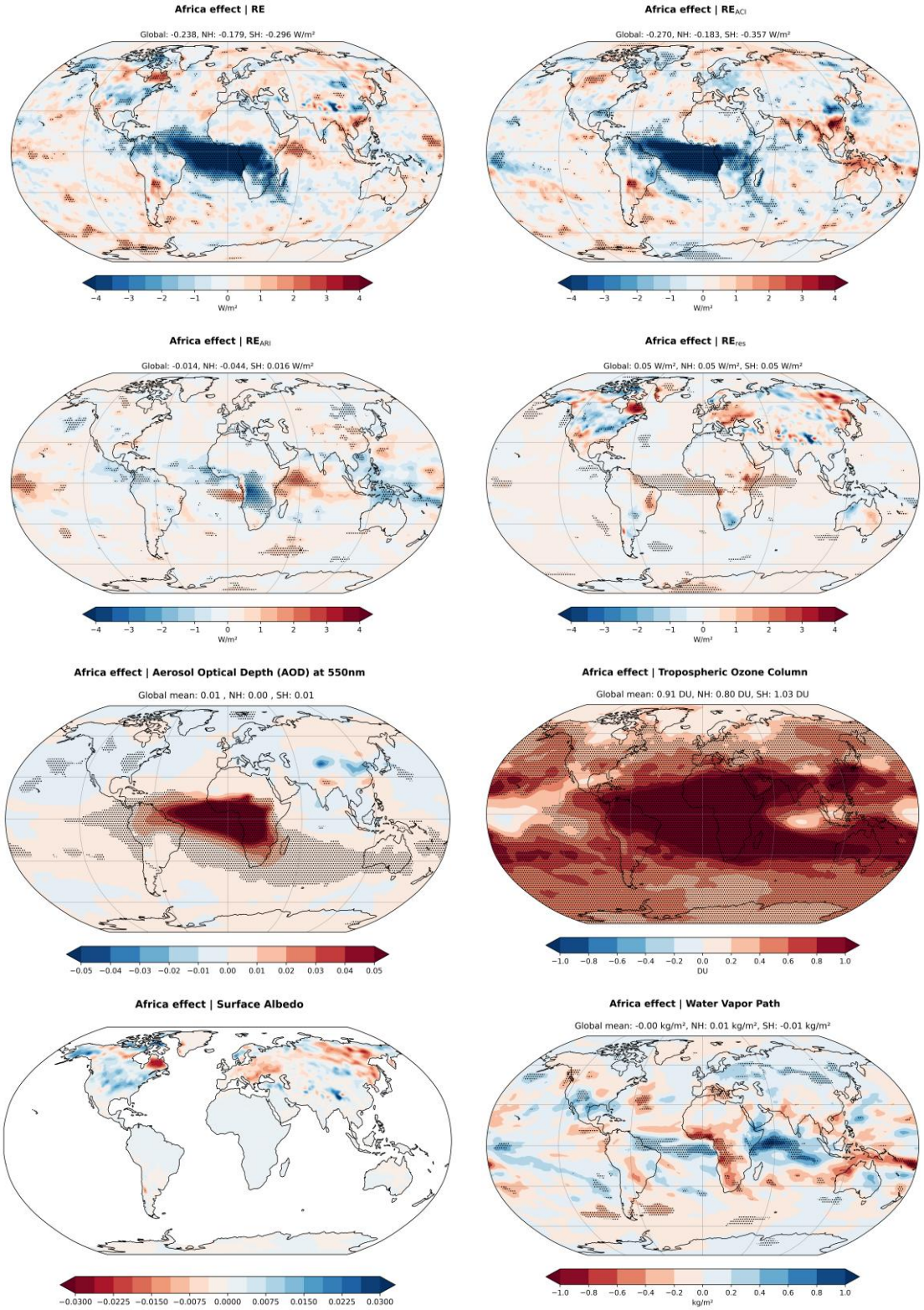

Figure S8: Spatial distribution of the Radiative Effect (RE) (W/m^2) of the present-day wildfire emissions from Africa (AF), and its decomposition into the RE due to the Aerosol-Radiation Interactions (RE$_{ARI}$), the Aerosol-Cloud Interactions (RE$_{ACI}$), and the residual term (RE$_{res}$). Moreover, the spatial distribution of the changes in Aerosol Optical Depth (AOD) at 500nm, the tropospheric O_3 (DU), the water vapor path (kg/m^2) and the surface albedo, are presented. The maps represent the difference between the 30-year mean of the atmosphere-only perturbation simulations and the 30-year mean of the simulations conducted without the AF emissions. Black stippling denotes that the change is significant at the 0.05 level. It is noted that in the present work, surface albedo is determined as (Surface Upwelling Shortwave Radiation)/(Surface Downwelling Shortwave Radiation)

- **Equatorial Asia (EQ) emissions effects**

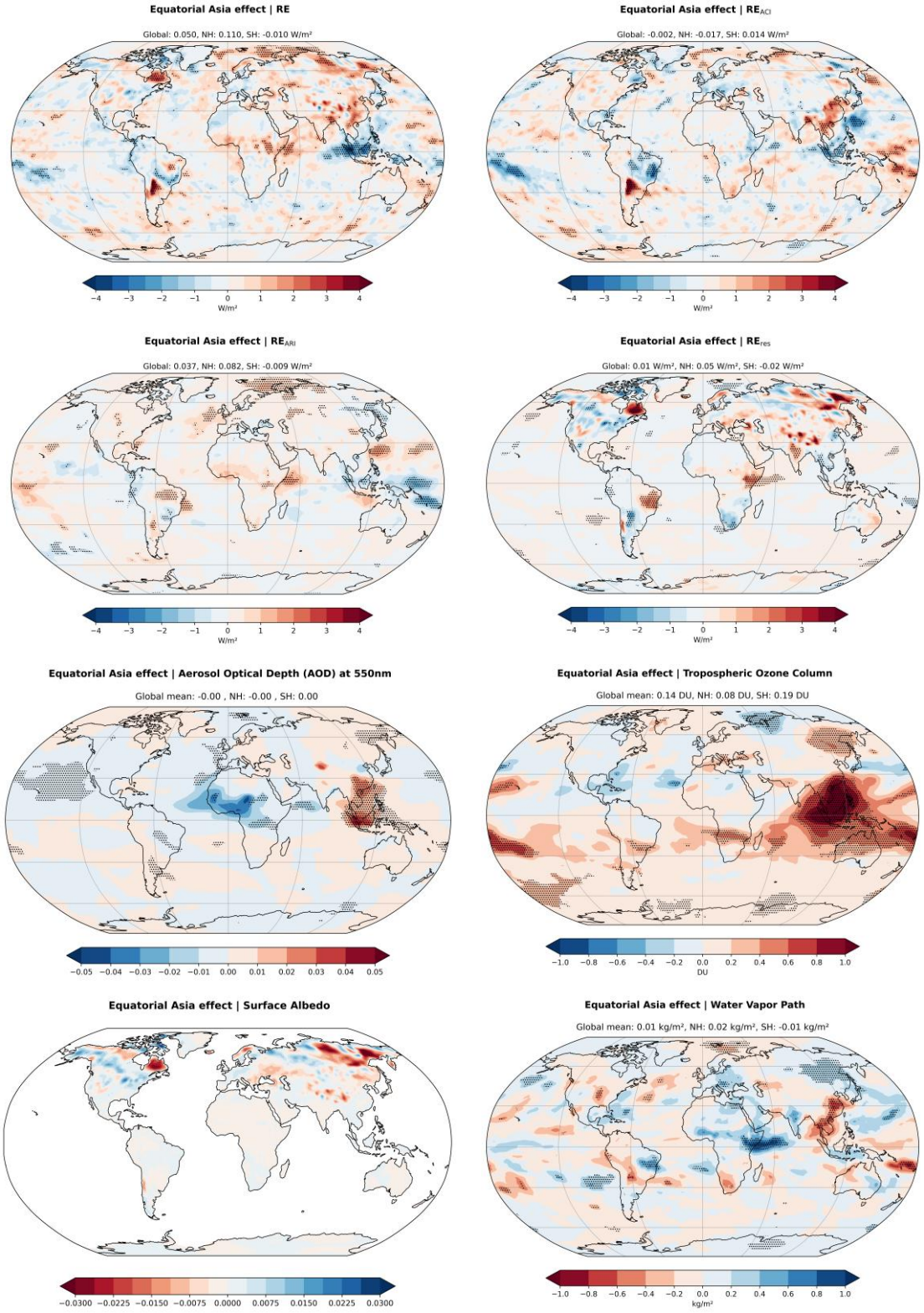

Figure S9: Spatial distribution of the Radiative Effect (RE) (W/m^2) of the present-day wildfire emissions from Equatorial Asia (EQ), and its decomposition into the RE due to the Aerosol-Radiation Interactions (RE_{ARI}), the Aerosol-Cloud Interactions (RE_{ACI}), and the residual term (RE_{res}). Moreover, the spatial distribution of the changes in Aerosol Optical Depth (AOD) at 500nm, the tropospheric O_3 (DU), the water vapor path (kg/m^2) and the surface albedo, are presented. The maps represent the difference between the 30-year mean of the atmosphere-only perturbation simulations and the 30-year mean of the simulations conducted without the EQ emissions. Black stippling denotes that the change is significant at the 0.05 level. It is noted that in the present work, surface albedo is determined as (Surface Upwelling Shortwave Radiation)/(Surface Downwelling Shortwave Radiation)

Regional wildfire emissions effects on global scale | Atmosphere-only simulations: Fast Precipitation responses

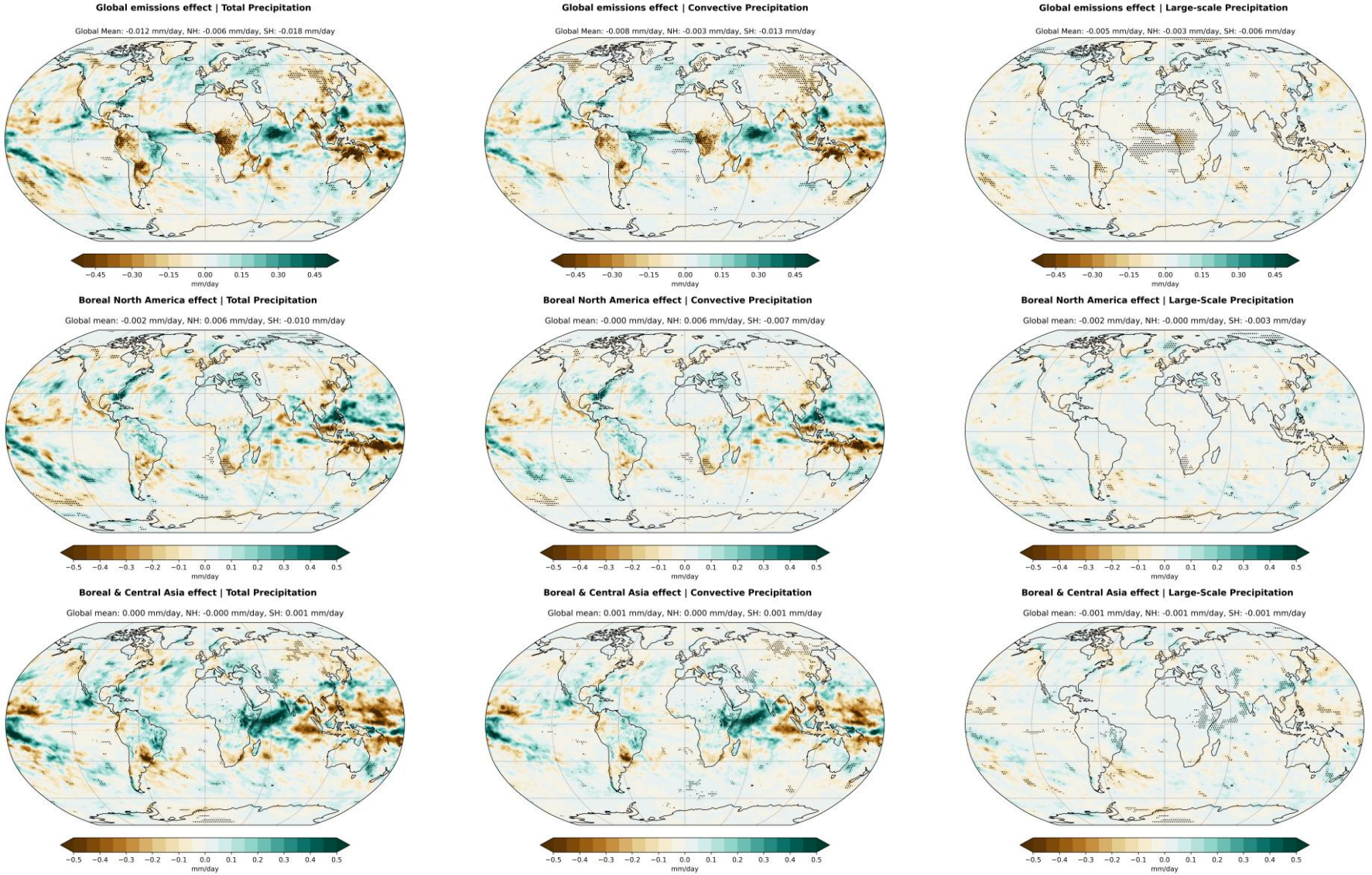

Figure S10: Spatial distribution of the changes in Total Precipitation (mm/day), Convective Precipitation and Large-scale Precipitation caused by the present-day wildfire emissions. Here, the effect of global wildfire emissions is presented, along with the effect the wildfire emissions from Boreal North America, Boreal & Central Asia, South America, Africa, and Equatorial Asia. The maps of the synergistic effect of the global wildfire emissions represent the difference between the 30-year mean of the atmosphere-only perturbation simulations and the 30-year mean of the control simulations, while the rest of the maps represent the difference between the 30-year mean of the perturbation simulations and the 30-year mean of the simulations conducted without the region of interest. Black stippling denotes that the change is significant at the 0.05 level.

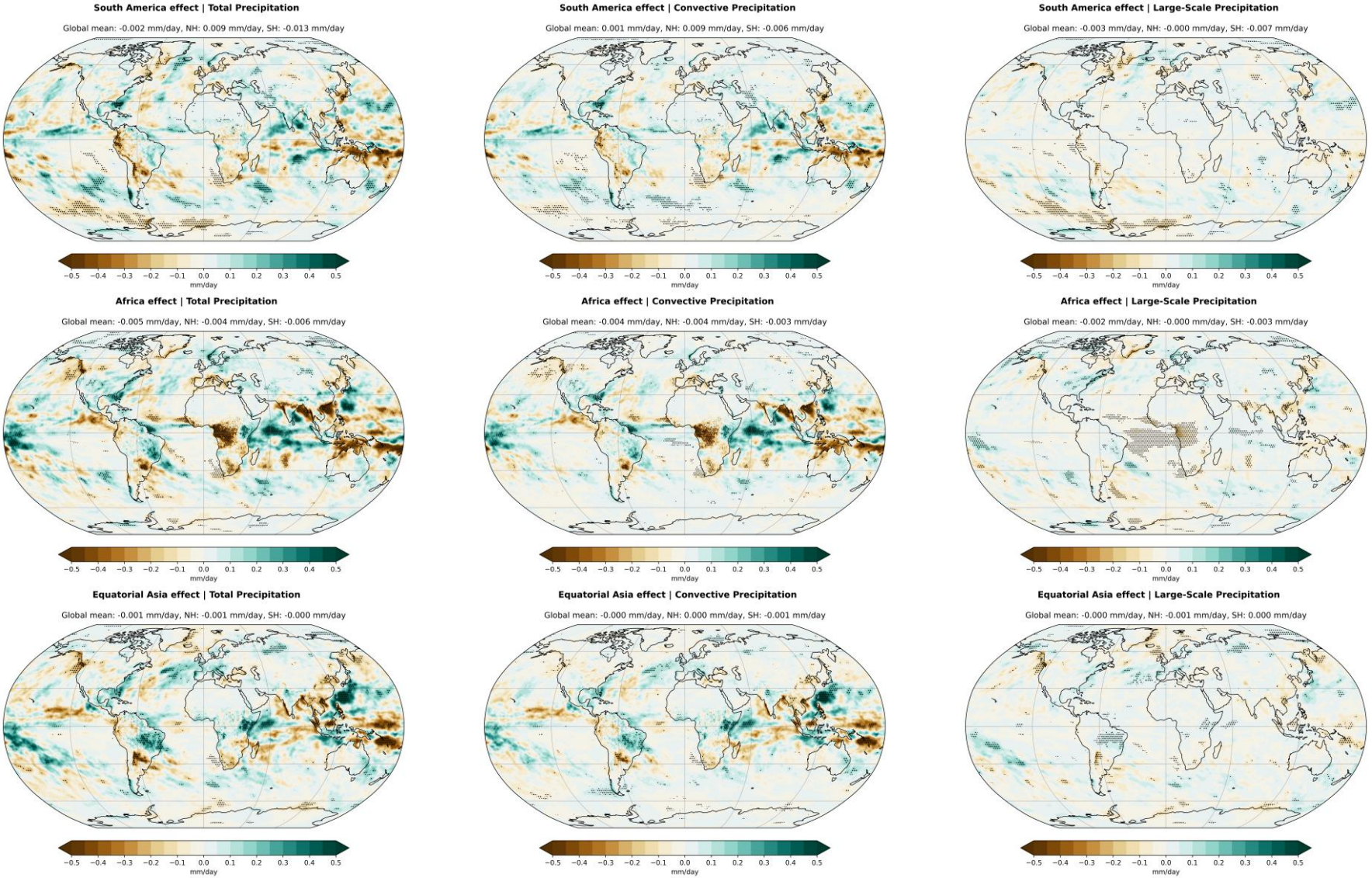

Figure S10: (continue) Spatial distribution of the changes in Total Precipitation (mm/day), Convective Precipitation and Large-scale Precipitation caused by the present-day wildfire emissions. Here, the effect of global wildfire emissions is presented, along with the effect the wildfire emissions from Boreal North America, Boreal & Central Asia, South America, Africa, and Equatorial Asia. The maps of the synergistic effect of the global wildfire emissions represent the difference between the 30-year mean of the atmosphere-only perturbation simulations and the 30-year mean of the control simulations, while the rest of the maps represent the difference between the 30-year mean of the perturbation simulations and the 30-year mean of the simulations conducted without the region of interest. Black stippling denotes that the change is significant at the 0.05 level.

Regional wildfire emissions effects on global scale | Atmosphere-only simulations: Fast Surface Temperature responses

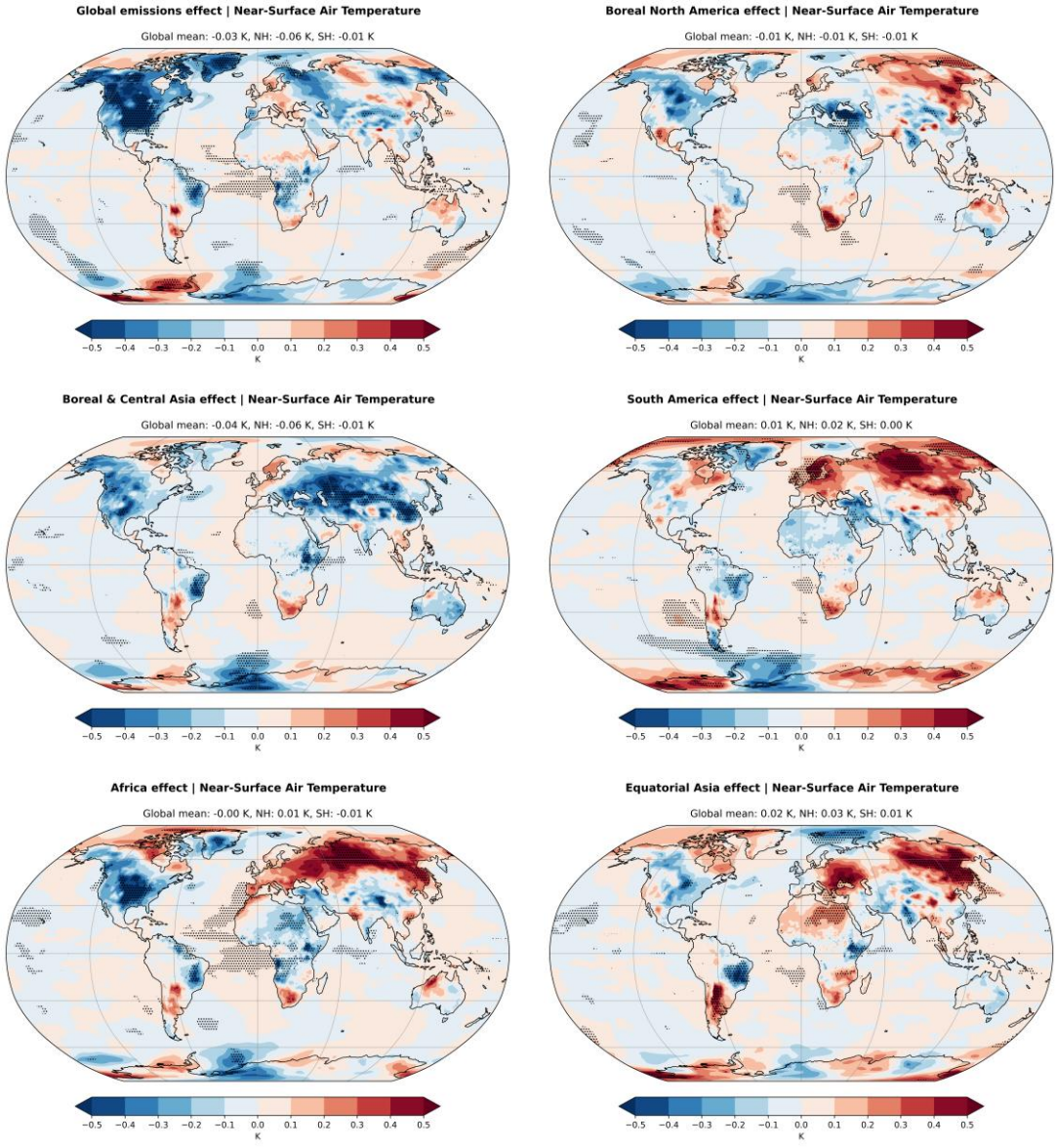

Figure S11: Spatial distribution of the changes in Near-Surface Temperature (K) caused by the present-day wildfire emissions. Here, the effect of global wildfire emissions is presented, along with the effect the wildfire emissions from Boreal North America, Boreal & Central Asia, South America, Africa, and Equatorial Asia. The maps of the synergistic effect of the global wildfire emissions represent the difference between the 30-year mean of the atmosphere-only perturbation simulations and the 30-year mean of the control simulations, while the rest of the maps represent the difference between the 30-year mean of the perturbation simulations and the 30-year mean of the simulations conducted without the region of interest. Black stippling denotes that the change is significant at the 0.05 level.

Regional wildfire emissions effects on global scale and global wildfire emissions synergistic effects | Atmosphere-only simulations: Surface upward latent heat flux

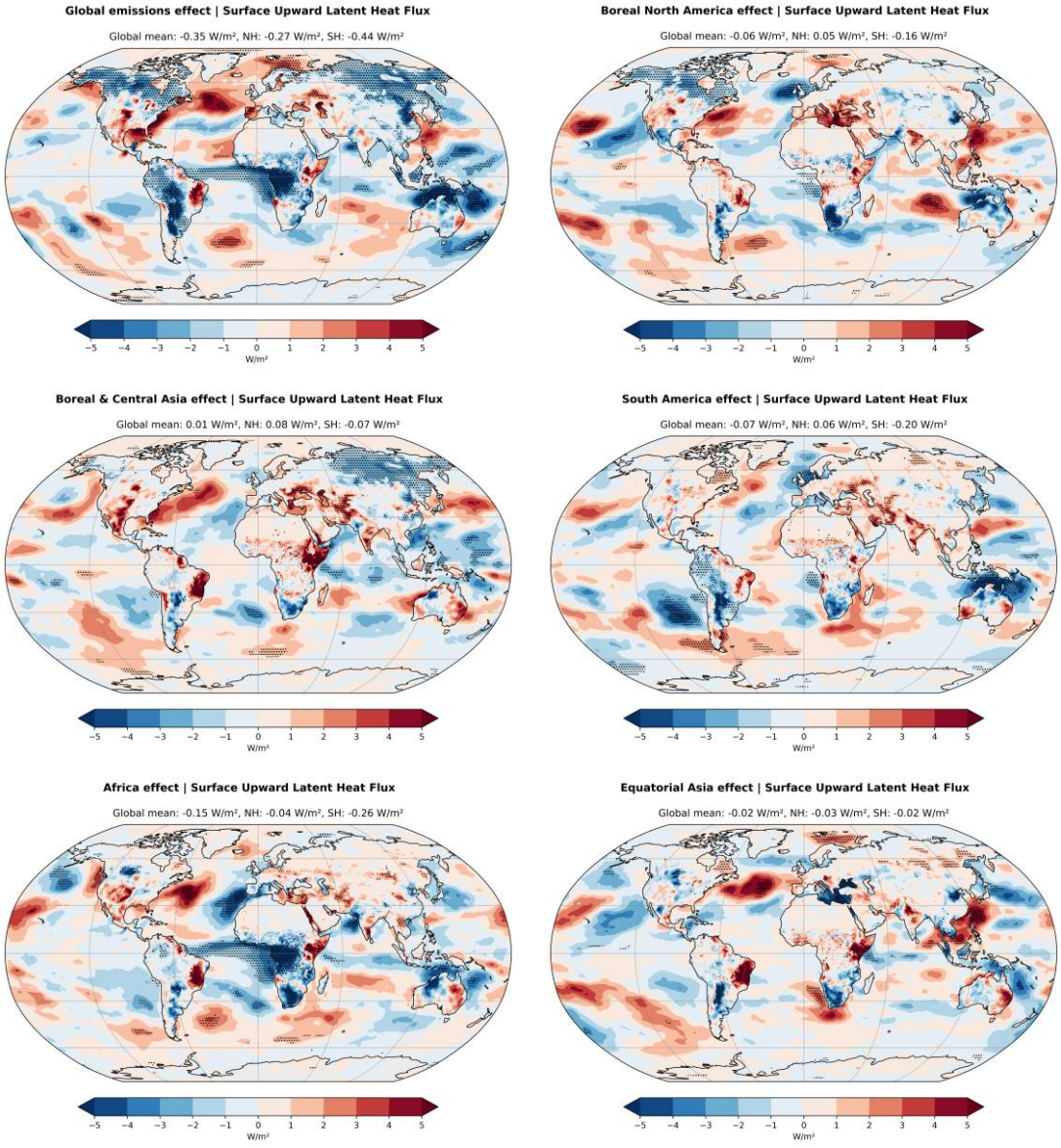

Figure S12: Spatial distribution of the changes in Surface Upward Latent Heat Flux (W/m^2) caused by the present-day wildfire emissions. Here, the effect of global wildfire emissions is presented, along with the effect the wildfire emissions from Boreal North America, Boreal & Central Asia, South America, Africa, and Equatorial Asia. The maps of the synergistic effect of the global wildfire emissions represent the difference between the 30-year mean of the atmosphere-only perturbation simulations and the 30-year mean of the control simulations, while the rest of the maps represent the difference between the 30-year mean of the perturbation simulations and the 30-year mean of the simulations conducted without the region of interest. Black stippling denotes that the change is significant at the 0.05 level.

Regional wildfire emissions effects on global scale and global wildfire emissions synergistic effects | Atmosphere-only simulations: Surface upward sensible heat flux

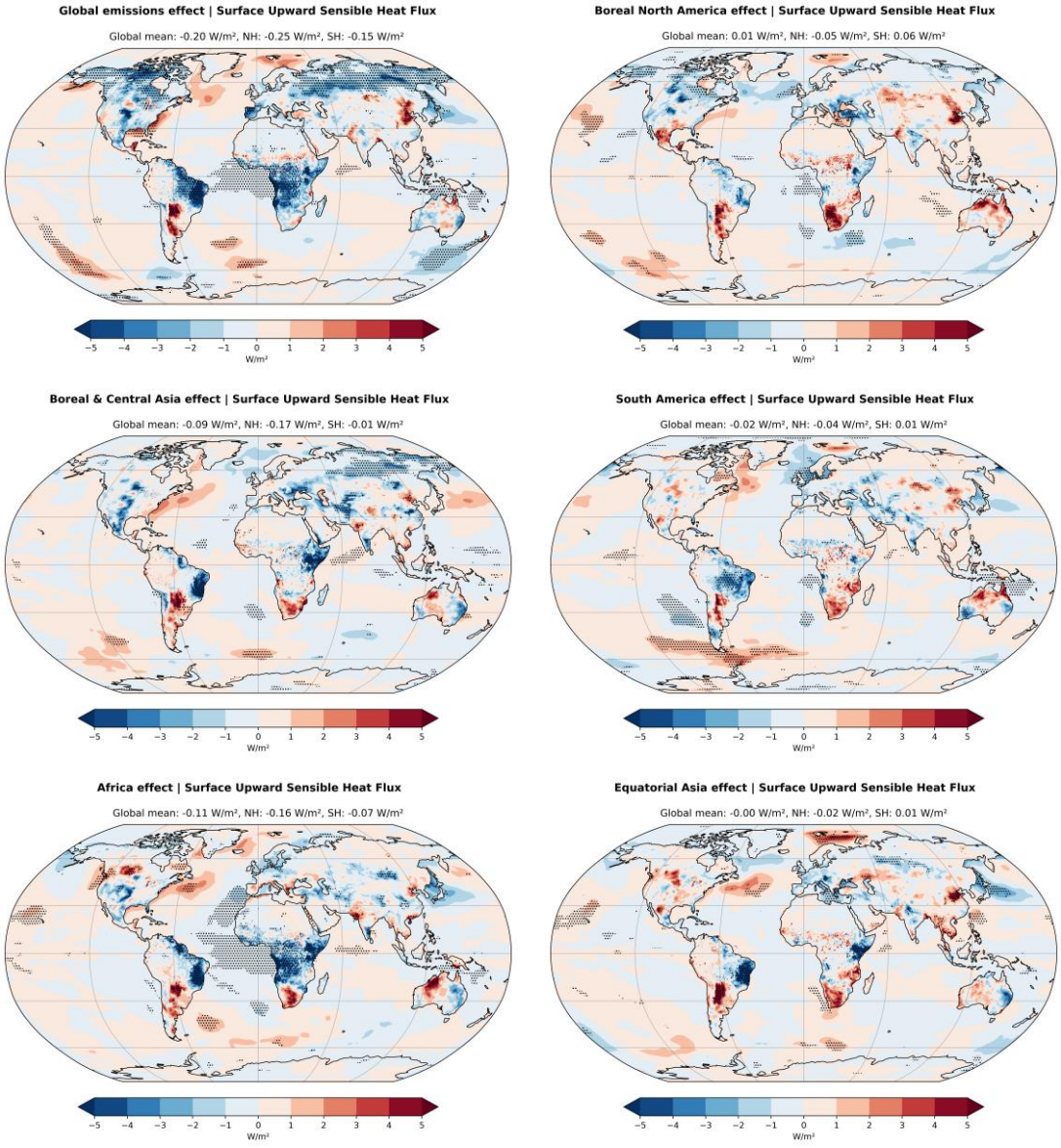

Figure S13: Spatial distribution of the changes in Surface Upward Sensible Heat Flux (W/m^2) caused by the present-day wildfire emissions. Here, the effect of global wildfire emissions is presented, along with the effect the wildfire emissions from Boreal North America, Boreal & Central Asia, South America, Africa, and Equatorial Asia. The maps of the synergistic effect of the global wildfire emissions represent the difference between the 30-year mean of the atmosphere-only perturbation simulations and the 30-year mean of the control simulations, while the rest of the maps represent the difference between the 30-year mean of the perturbation simulations and the 30-year mean of the simulations conducted without the region of interest. Black stippling denotes that the change is significant at the 0.05 level.

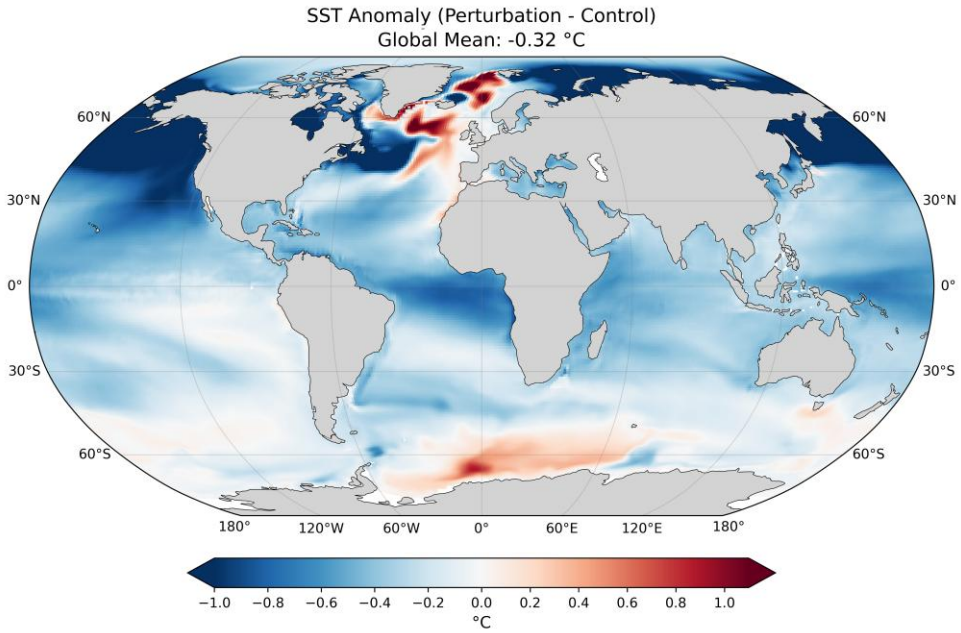

Figure S14: Spatial distribution of the Sea surface Temperatures (SSTs) changes due to the present-day wildfire emissions. The maps represent the difference between the 50-year mean of the fully coupled ocean-atmosphere perturbation simulations and the 35-year mean of the corresponding control simulations.

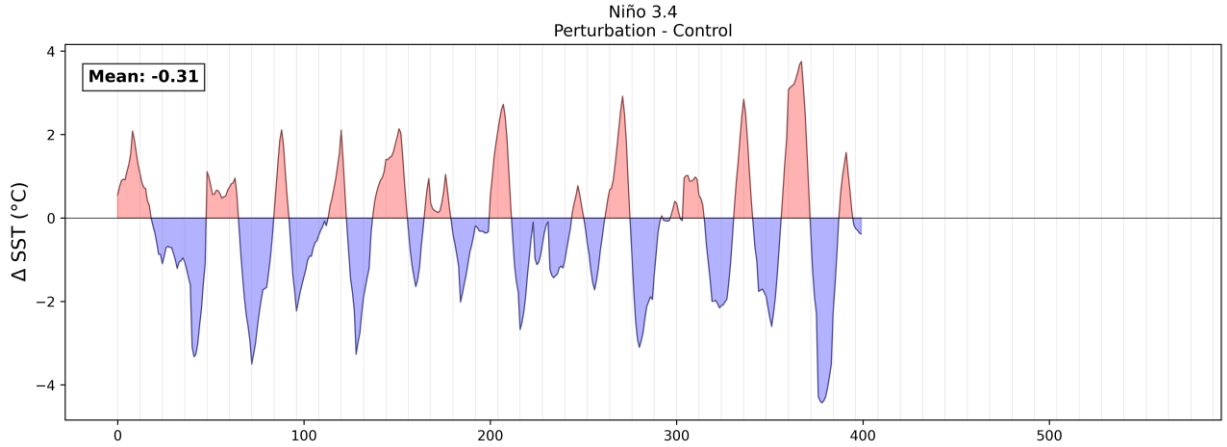

Figure S15: ENSO oceanic index Niño 3.4 (5-month rolling mean) calculated as the difference between the perturbation run and control run (50 years of fully coupled ocean-atmosphere simulations), and as presented in Trenberth (2025a)

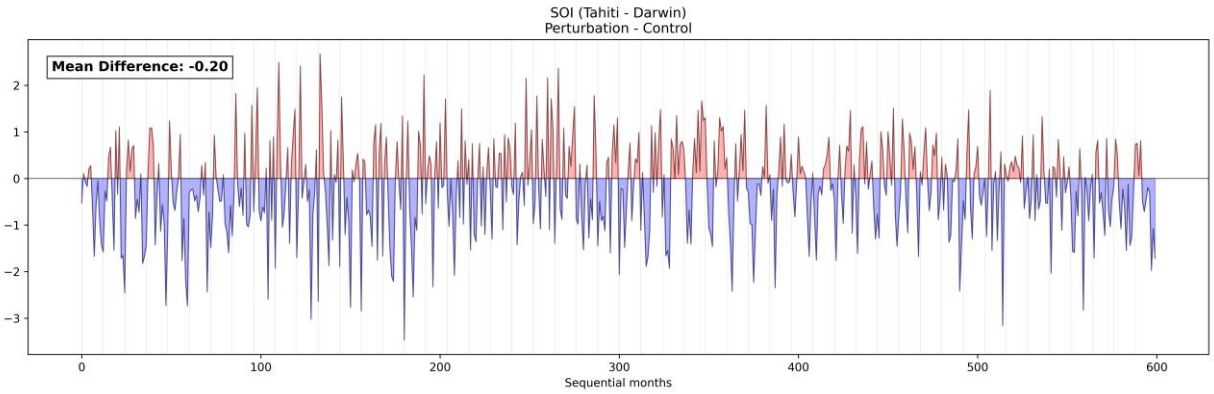

Figure S16: ENSO atmospheric index SOI (Southern Oscillation Index) calculated as the difference between the perturbation run and control run (50 years of fully coupled ocean-atmosphere simulations), adopting the methodology presented in Trenberth (2025b)

Supplementary Material References

Feng, L., Smith, S. J., Braun, C., Crippa, M., Gidden, M. J., Hoesly, R., Klimont, Z., van Marle, M., van den Berg, M., & van der Werf, G. R. (2020). The generation of gridded emissions data for CMIP6. Geoscientific Model Development, 13(2), 461–482. https://doi.org/10.5194/gmd-13-461-2020

Trenberth, K. & National Center for Atmospheric Research Staff (Eds). (2025a) Last modified 2025-12-11 "The Climate Data Guide: Nino SST Indices (Nino 1+2, 3, 3.4, 4; ONI and TNI)." Retrieved on 2026-04-02 from https://climatedataguide.ucar.edu/climate-data/nino-sst-indices-nino-12-3-34-4-oni-and-tni

Trenberth, K. & National Center for Atmospheric Research Staff (Eds). (2025b) Last modified 2025-12-11 "The Climate Data Guide: Southern Oscillation Indices: Signal, Noise and Tahiti/Darwin SLP (SOI)." Retrieved on 2026-04-02from https://climatedataguide.ucar.edu/climate-data/southern-oscillation-indices-signal-noise-and-tahitidarwin-slp-soi